

Comparing ERA-40 based L-band  
brightness temperatures with  
Skylab observations: A calibration /  
validation study using the  
Community Microwave Emission  
Model

M. Drusch, T. Holmes, P. de Rosnay,  
G. Balsamo

Research Department

ECMWF, UK

Accepted by Hydrometeorology

July 2008

*This paper has not been published and should be regarded as an Internal Report from ECMWF.  
Permission to quote from it should be obtained from the ECMWF.*



European Centre for Medium-Range Weather Forecasts  
Europäisches Zentrum für mittelfristige Wettervorhersage  
Centre européen pour les prévisions météorologiques à moyen terme

Series: ECMWF Technical Memoranda

A full list of ECMWF Publications can be found on our web site under:

<http://www.ecmwf.int/publications/>

Contact: [library@ecmwf.int](mailto:library@ecmwf.int)

©Copyright 2008

European Centre for Medium-Range Weather Forecasts  
Shinfield Park, Reading, RG2 9AX, England

Literary and scientific copyrights belong to ECMWF and are reserved in all countries. This publication is not to be reprinted or translated in whole or in part without the written permission of the Director. Appropriate non-commercial use will normally be granted under the condition that reference is made to ECMWF.

The information within this publication is given in good faith and considered to be true, but ECMWF accepts no liability for error, omission and for loss or damage arising from its use.

## Abstract

The community microwave emission model (CMEM) has been used to compute global L-band brightness temperatures at the top of the atmosphere. The input data comprise surface fields from ECMWF's 40-year Re-Analysis (ERA-40), vegetation data from the ECOCLIMAP data set, and the Food and Agriculture Organization (FAO) soil data base. Modelled brightness temperatures have been compared against (historic) observations from the S-194 passive microwave radiometer onboard the Skylab space station. Different parameterizations for surface roughness and the vegetation optical depth have been used to calibrate the model. The best results have been obtained for rather simple approaches proposed by [Wigneron et al. \(2001\)](#) and [Kirdyashev et al. \(1979\)](#). The rms errors after calibration are 10.7 K and 9.8 K for North and South America, respectively. Comparing the ERA-40 soil moisture product against the corresponding in-situ observations suggests that the uncertainty in the modelled soil moisture is the predominant contributor to these rms errors. Although the bias between model and observed brightness temperatures are reduced after the calibration, systematic differences in the dynamic range remain. For NWP analysis applications bias-correction schemes should be applied prior to data assimilation. The calibrated model has been used to compute a 10-year brightness temperature climatology based on ERA-40 data.

## 1 Introduction

Satelliteborne passive microwave observations at L-band will become routinely available for the first time through the European Space Agency's (ESA) Soil Moisture and Ocean Salinity mission (SMOS) foreseen in 2009. The sensitivity of L-band measurements to soil moisture has been thoroughly analysed (e.g. [Ulaby et al. \(1986\)](#)) and the applicability of soil moisture retrievals has been demonstrated over the last decades (e.g. [Jackson et al. \(1999\)](#)). In recent years, data assimilation studies also demonstrated the potential benefit of this observation type for hydrological modelling (e.g. [Reichle and Koster \(2005\)](#)) and Numerical Weather Prediction (NWP; e.g. [Balsamo et al. \(2007\)](#), [Drusch \(2007\)](#)).

For NWP centres SMOS data will be most beneficial for the soil moisture analysis, which is used to initialize operational weather forecasts. For the atmospheric and surface analyses the medium-range forecast system at ECMWF receives observations within 3 hours of sensing. The analyses are then produced within 1.5 hours to guarantee a timely start of the forecast computations and to minimize the latency between forecast initialization and forecast dissemination times ([Haseler \(2004\)](#)). For short-range forecasts and now-casting the operational production schedule can be even tighter. The operational constraints have a significant influence on the design of the data assimilation system and how a specific data set can be used.

Producing the SMOS Level 2 soil moisture product will take more than 24 hours but brightness temperatures will be available in Near Real Time (NRT, i.e. within 3-hours of sensing). Consequently, a land surface microwave emission model is needed to transfer the model state variables (e.g. soil moisture, soil temperature, etc.) into observation space (brightness temperature). Auxiliary data sets (e.g. soil temperature, profiles of atmospheric temperature and relative humidity) used for this computation are also required in NRT and should be consistent with the first guess state variables. In the current operational data assimilation system approximately 18 million satellite observations are used and the radiative transfer calculations for the model first guess are based on short-range forecasts.

Due to the limited time available and the high computational costs of an advanced variational data assimilation system, operational analyses are often produced at a low spatial resolution. Although the ECMWF medium-range forecast is currently produced at  $\simeq 25$  km resolution the atmospheric 4D-Var analysis is based on analysis increments with  $\simeq 120$  km resolution. It is likely that the surface analysis system will be operated at a similar reduced resolution.

In this study, we compare modelled brightness temperatures based on ECMWF's 40-year reanalysis (ERA-40)

and observations from the Skylab satellite mission in 1973. The ERA-40 land surface scheme is comparable to the current version used in the Integrated Forecast System (IFS) and its spatial resolution matches that of the data assimilation system. The SKYLAB data set is limited and comprises only nine overpasses. However, these observations are the only spaceborne L-band data available. It should be noted that they cover a large variety of landscapes, vegetation types and climates. In addition, the measurements were taken during different seasons. As a consequence, we have to wait at least half a year after launch to get calibrated SMOS observations covering a similar period; the operational data monitoring should start much earlier.

Skylab data are briefly introduced in section 2. In sections 3 and 4 we introduce the the Community Microwave Emission Model (CMEM) and the operational NWP data sets used in the future SMOS based soil moisture analysis. To provide a timely calibration and validation benchmark for adaptation to SMOS, the model is calibrated using the Skylab observations. Systematic and random model errors which have to be known for data assimilation are quantified and discussed (section 5). Based on ERA-40 data a L-band climatology for the period from 1990 to 2000 is produced and discussed in section 7.

## 2 Skylab S-194 Observed Brightness Temperatures

The NASA Skylab mission was a first example of a space station. It operated between May 1973 and July 1977 on a polar orbit at 435 km nominal altitude; the orbit period was 93 minutes. The Skylab S-194 instrument was a nadir viewing passive microwave radiometer operating at 1.4 GHz with a hard mounted antenna. The resolution of a single observation was approximately 110 km, the distance between the centres of two consecutive footprints was 2.5 km. The sensor calibration was based on fixed cold and hot load inputs and the absolute antenna temperature was obtained with an accuracy of 1 K (Eagleman and Lin (1976)).

Collecting data from S-194 required the astronauts onboard the satellite. Consequently, the number of observations is limited to the following periods: 14 May - 22 June 1973, 28 June - 25 September 1973, and 16 November 1973 - 8 February 1974. The S-194 data and a comprehensive description are now available under <http://disc.gsfc.nasa.gov> (Jackson et al. (2004)).

In total, nine tracks of observations are available (Fig. 1). Although the number of observations is quite limited it should be emphasized that a large variety of landscapes, vegetation types, climates and seasons is covered. This spatial coverage could hardly be achieved from airborne field campaigns and consequently the S-194 measurements is the best data set available to perform a first calibration of land surface emission models at L-band for global NWP applications.

## 3 The Community Microwave Emission Model

Land surface emission modelling in NWP centres relies mainly on results published in the peer reviewed literature due to practical constraints on resources. As a consequence there is a substantial latency between the latest developments and their beneficial impact on operational applications. In addition, feedback from operational users to the various research groups developing algorithms and parameterizations is often difficult to obtain.

ESA's Calibration, Validation and Retrieval Study provides the framework for a timely and direct exchange of information between the SMOS Validation and Retrieval Team (SVRT) members working on parameterizations and forward modelling problems, the NWP community and ESA. CMEM is the appropriate common tool for emission model developments and applications. The detailed CMEM documentation and the source code can be obtained from [http://www.ecmwf.int/research/ESA\\_projects/SMOS/cmem/cmem.index.html](http://www.ecmwf.int/research/ESA_projects/SMOS/cmem/cmem.index.html).

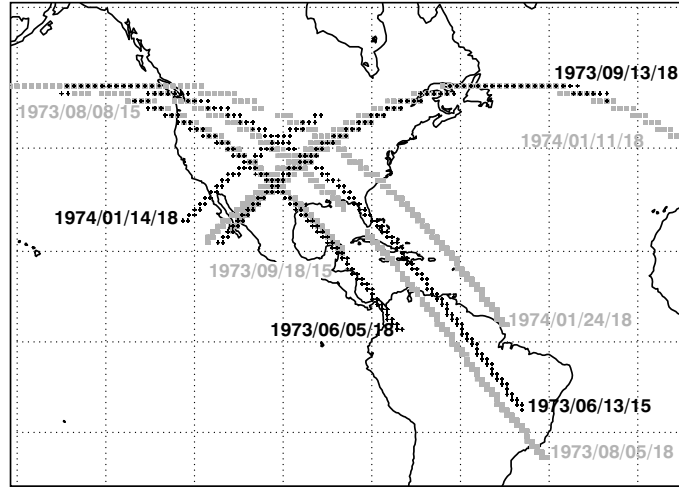


Figure 1: Spatial and temporal coverage of the Skylab S-194 observations with the corresponding observation dates and overpass time (UTC). Black tracks have been used for the calibration. The validation has been based on the grey tracks.

CMEM comprises the physics and parameterizations used in the Land Surface Microwave Emission Model (LSMEM; [Drusch et al. \(2001\)](#)) and the L-band Microwave Emission of the Biosphere (L-MEB; [Wigneron et al. \(2007\)](#)). It is based on a simplified solution for the vector radiative transfer equation (e.g. [Kerr and Njoku \(1990\)](#), [Drusch and Crewell \(2005\)](#)). For polarization  $p$  the brightness temperature over snow free areas at the Top Of the Atmosphere (TOA)  $T_{Btoa,p}$  can be expressed as:

$$T_{Btoa,p} = T_{Bau,p} + \exp(-\tau_{atm,p}) \cdot T_{Btov,p} \quad (1)$$

and

$$\begin{aligned} T_{Btov,p} &= T_{Bsoil,p} \cdot \exp(-\tau_{veg,p}) \\ &+ T_{Bveg,p} (1 + r_{r,p} \cdot \exp(-\tau_{veg,p})) \\ &+ T_{Bad,p} \cdot r_{r,p} \cdot \exp(-2 \cdot \tau_{veg,p}) \end{aligned} \quad (2)$$

where  $T_{Bau,p}$  is the up-welling atmospheric emission and  $\tau_{atm,p}$  is the atmospheric optical depth.  $T_{Btov,p}$  is the top of vegetation brightness temperature when the vegetation is represented as a single-scattering layer above a rough surface.  $T_{Bsoil,p}$ ,  $T_{Bveg,p}$  and  $T_{Bad,p}$  are the soil, vegetation layer and downward atmospheric contributions, respectively.  $r_{r,p}$  is the soil reflectivity of the rough surface (one minus the emissivity  $e_{r,p}$ ) and  $\tau_{veg,p}$  is the vegetation optical depth along the viewing path. Snow is represented through the HUT snow emission model ([Pulliainen et al. \(1999\)](#)) as a single additional homogeneous snow layer with low attenuation and an additional dielectric boundary.

CMEM comprises four modules for computing the contributions from soil, vegetation, snow and the atmosphere. The code is designed to be highly modular and for each microwave modelling component, a choice of several parameterizations are considered. Table 1 summarizes the modular structure and lists the options provided in CMEM. The following paragraphs address surface roughness and vegetation contribution since these components have been used for the calibration of the model.

[Wang and Choudhury \(1981\)](#) propose a semi-empirical approach to represent soil roughness effects on the microwave emission. The rough emissivity is computed as a function of the smooth emissivity and three parameters  $Q$ ,  $h$ ,  $N$ :

$$r_{r,p} = (Q \cdot r_{s,p} + (1 - Q) \cdot r_{s,q}) \cdot \exp(-h \cdot \cos^N \psi) \quad (3)$$

Table 1: Modular configuration of CMEM. For each component, the key variable is indicated and the list of options is provided. The soil module includes 4 components: the dielectric mixing model ( $\epsilon$ ), the effective temperature model ( $T_{eff}$ ), the smooth surface emissivity model ( $e_{s,p}$ ), the rough surface emissivity,  $e_{r,p}$ . For each of them several parameterizations are proposed. The vegetation module key variable is the vegetation optical thickness  $\tau_{veg,p}$ . The snow module computes the snow reflectivity  $rsn_p$  and the atmospheric module provides the atmosphere optical thickness  $\tau_{atm,p}$ . Options in bold are those used in this paper.

Module	Output	Parameterizations		
Soil	$\epsilon$	<b>Dobson et al. (1985)</b>	Mironov et al. (2004)	Wang and Schmugge (1980)
	$T_{eff}$	Choudhury et al. (1982)	Holmes et al. (2006)	<b>Wigneron et al. (2001)</b>
	$e_{s,p}$	<b>Fresnel</b>	Wilheit (1978)	
	$e_{r,p}$	Choudhury et al. (1979)	SMOS ATBD (2007)	Wegmüller and Mätzler (1999)
Vegetation	$\tau_{veg,p}$	<b>Wigneron et al. (2007)</b>	<b>Wigneron et al. (2001)</b>	
		<b>Jackson and Schmugge (1991)</b>	<b>Kirdyashev et al. (1979)</b>	Wegmüller et al. (1995)
Snow	$rsn_p$	<b>Pulliaminen et al. (1999)</b>		
Atmosphere	$\tau_{atm,p}$	Liebe (2004)	<b>Pellarin et al. (2003)</b>	Ulaby et al. (1986)

where  $p$  and  $q$  refer to the polarization states,  $Q$  is the polarization mixing factor,  $N$  describes the angular dependence,  $h$  is the roughness parameter and  $\psi$  the incidence angle. The mixing factor  $Q$  is considered to be very low at low frequencies and is generally set to 0 (Wigneron et al. (2007); Njoku et al. (2003)).

For the roughness parameter  $h$  a number of parameterizations exist. They are based on (i) empirical coefficients, wave number, and the rms surface height  $\sigma$  (Choudhury et al. (1979), Wegmüller and Mätzler (1999)), (ii) empirical coefficients, wave number, the rms surface height and correlation length (Wigneron et al. (2001)), (iii) soil moisture and soil texture (SMOS ATBD (2007)), or (iv) soil moisture and vegetation type (Wigneron et al. (2007)).

In CMEM vegetation is represented through  $\tau - \omega$  approaches in which the vegetation layer has a direct contribution to the TOA signal and attenuates the emission from the underlying soil:

$$T_{Bveg,p} = T_c \cdot (1 - \omega_p) \cdot (1 - \exp(-\tau_{veg,p})) \quad (4)$$

where  $T_c$  is the canopy temperature and  $\omega_p$  is the single scattering albedo at polarization  $p$ .

Based on Eq. 4, Jackson and Schmugge (1991) propose a simple parameterization to compute the vegetation optical thickness:

$$\tau_{veg,p} = b \cdot \frac{VWC}{\cos\psi} \quad (5)$$

where  $b$  and  $VWC$  are the vegetation structure parameter and the vegetation water content, respectively. The single scattering albedo is assumed constant at  $\omega = 0.05$  for low vegetation types (grass and crops) and for high vegetation types (forests).

The Wigneron et al. (2007) vegetation optical thickness model also describes the vegetation effect with Eq. 4. In their formulation the single scattering albedo depends on vegetation type and polarization. The polarized optical thickness is expressed as:

$$\tau_{veg,p} = \tau_{nadir} \cdot (\cos^2\psi + tt_p \sin^2\psi) \frac{1}{\cos\psi} \quad (6)$$

$$\tau_{nadir} = b' \cdot LAI + b'' \quad \text{for low vegetation} \quad (7)$$

$$\tau_{nadir} = b''' \quad \text{for high vegetation} \quad (8)$$

where  $tt_p$  parameters represent the angular effect on vegetation optical thickness for each polarization and

vegetation types (at nadir  $tt_p$  has no effect on the simulations). The vegetation structure parameters  $b'$ ,  $b''$  and  $b'''$  and the single scattering albedo are obtained from a lookup tables (Wigneron et al. (2007)).

The Kirdyashev et al. (1979) parameterization expresses the vegetation optical thickness as a function of the wave number  $k$  (between 1 GHz and 7.5GHz), the dielectric constant of saline water,  $\epsilon''_{sw}$  (imaginary part), WVC, incidence angle  $\psi$ , water density  $\rho_{water}$  and a vegetation structure parameter  $a_{geo}$ :

$$\tau_{veg,p} = a_{geo} \cdot k \cdot \frac{WVC}{\rho_{water}} \cdot \epsilon''_{sw} \cdot \frac{1}{\cos\psi} \quad (9)$$

Again, the single scattering albedo is assumed constant at  $\omega = 0.05$ .

$T_{B_{tov,p}}$  is computed for each model grid box taking the sub-grid scale variability of the land surface into account. Up to seven tiles can be considered in each CMEM grid box: Bare soil, low vegetation, high vegetation (each are either free of snow or snow-covered), and open water. For the vegetation tiles the dominant vegetation class is obtained from an auxiliary land use classification data set. The grid box averaged brightness temperature is computed using the weighted sum of the brightness temperatures obtained for the individual tiles.

## 4 CMEM Input Data and Calibration Strategy

The calibration of a complex model system is often an ill-posed problem since the number of parameters exceeds the number of observations at a given location. Therefore, it is essential to focus on the key parameters in the emission modelling process. Jones et al. (2004) ranked the main variables and parameters entering passive microwave land surface emission models according to their impact on  $TB_{toa}$ . The number in the brackets are the relative impact (with respect to soil moisture) as defined through the normalized perturbation response given in Jones et al. (2004): Volumetric soil moisture (1.0), vegetation water content (0.63), soil roughness parameter (0.30), vegetation structure coefficient (0.18), effective soil temperature (0.13), vegetation single scattering albedo (0.08), soil bulk density (0.05), vegetation temperature (0.03), and soil texture (0.01). Although these values are strictly valid at C- and X-band they can give an indication of the relative importance of the individual parameters at L-band. In the following paragraphs we discuss the availability and accuracy of the key products entering the land surface emission model. A summary on the input parameters is given in Tab. 2. It should

Table 2: CMEM input parameters. The relative impact has been derived from the normalized perturbation response at C- and X-band given in Jones et al. (2004). We distinguish between three types of parameter values: (i) dynamic - NWP model output varying in space and time, (ii) static - a data base representing parameters with a limited spatial and / or temporal variability, and (iii) constant - a single value. WVC is obtained from ECOCLIMAP LAI using Pellarin et al. (2003); soil bulk densities have been derived from the FAO soil texture data set following Hillel (1980). Parameters that are used to calibrate CMEM are described in Tab. 3.

Variable	Description	Relative Impact	Value	Source	Reference
$\theta$	vol. soil moisture	1.0	dynamic	ERA-40	Uppala et al. (2005)
WVC	veg. water content	0.63	static	ECOCLIMAP	Masson et al. (2003)
$T_{eff}$	eff. soil temperature	0.13	dynamic	ERA-40	Uppala et al. (2005)
$\omega$	veg. single scattering albedo	0.08	constant	—	Holmes et al. (2008)
—	soil bulk density	0.05	static	FAO	FAO (2000)
$T_c$	vegetation temperature	0.03	dynamic	ERA-40	Uppala et al. (2005)
—	soil texture	0.01	static	FAO	FAO (2000)
—	snow water equivalent	na	dynamic	ERA-40	Uppala et al. (2005)
—	snow density	na	dynamic	ERA-40	Uppala et al. (2005)

be noted that our focus lies on global near real time applications. For hindcast, re-analyses and soil moisture retrievals better products may be available, especially on local to regional scales.

*Volumetric soil moisture* ( $\theta$ ) is routinely analysed in NWP systems and is directly linked to soil, vegetation, and atmospheric parameters. For this study,  $\theta$  is obtained from the ERA-40 reanalysis data set (Uppala et al. (2005)). The observations used in the analysis comprise various satellite data sets as well as ground based measurements and conventional synoptic data. These data sets were assimilated through a 3D-Var analysis scheme making use of the IFS at T159 spectral resolution ( $\sim 1.125^\circ$  horizontal spacing) with 60 vertical levels. The surface scheme within the IFS is the Tiled ECMWF Scheme for Surface Exchanges over Land (TESSEL) as described in van den Hurk et al. (2000). The soil is discretized in four layers of 0.07, 0.21, 0.72, and 1.89 m depth (from top to bottom). We use the soil moisture analysed for the first model layer representing a depth of 0.07 m.

*Vegetation water content* (VWC) is not used by the NWP model and is poorly known on large spatial scales. A number of empirical formulas exist which relate vegetation water content to the Normalized Difference Vegetation Index or Leaf Area Index from satellite data like AVHRR (Advanced Very High Resolution Radiometer) or MODIS (Moderate Resolution Imaging Spectroradiometer) (e.g. Jackson et al. (1999)). However, vegetation data sets from optical instruments are not available in near real time and NWP centres have just started to explore the capabilities of offline LAI analysis systems (e.g. Jarlan et al. (2008)). Currently, static vegetation data sets are used by the NWP community and VWC has been derived from the ECOCLIMAP LAI data set (Masson et al. (2003)) following Pellarin et al. (2003):

$$VWC = 0.5 \cdot LAI \quad (10)$$

for grasslands and crops; the vegetation water content for rain forest, deciduous forests and coniferous forests has been set to 10, 4 and  $3 \text{ kg m}^{-2}$  (Holmes et al. (2008)), respectively, for the first guess model calibration setup. However, these values have not been validated on the continental scale and represent the branch water content rather than the entire biomass. In this study we consider the vegetation water content of forests as a calibration parameter.

The brightness temperatures at the top of the atmosphere also depend on the *effective soil temperature* ( $T_{eff}$ ) and *canopy temperature* ( $T_c$ ). The effective temperature depends on the vertical profile of soil temperature close to the surface; it has been parameterized following Wigneron et al. (2001) using ERA-40 soil temperatures. We also use ERA-40 soil temperature fields at 0.035 m depth as an approximation for canopy temperatures. Since the influence of these parameters on the brightness temperature is comparably low (Jones et al. (2004)) these approximations do not introduce a substantial error.

*Soil texture* data from FAO (Food and Agriculture Organization) are static at 10 km spatial resolution and distinguish between three soil texture classes (coarse, medium, fine) (FAO (2000)). Sand and clay fractions have been computed from a look-up table according to Salgado (1999). The 10 km data sets have then been aggregated to T159 spectral resolution.

*Snow water equivalent* data and snow density have also been obtained from the ERA-40 data set. The reanalysis is based on a short-range weather forecast and in-situ observations (Drusch et al. (2004b)); fractional snow coverage is set to 100 % in the presence of snow.

*Open water* (i.e. lakes, rivers, flood areas, etc.) represents a challenge for soil moisture retrievals as well as for data assimilation applications (Gao et al. (2006)). Global NRT data sets for surface temperatures do not exist and the emission of rough water surfaces is difficult to estimate. For the future soil moisture analysis observations with open water fractions exceeding 5 % will be flagged and excluded. For this study, soil temperature has been used as a proxy for lake and sea temperature. The salinity of open water in a land pixel is set to 0 psu, for sea pixels the salinity is 32.5 psu. Using the Klein and Swift (1977) parameterization for the dielectric constant of saline water Fresnel reflectivities of  $\sim 0.6$  have been obtained from these values.

*Soil roughness, vegetation structure coefficient, and vegetation water content* for dense vegetation are used for

the emission modelling only. They do not feed back into the NWP model or only indirectly and are poorly known on large spatial scales. For the calibration process we tune these parameters and we use different parameterizations for the rough surface reflectivity and the vegetation opacity. A discussion on other error sources will be given in section 6.

The setup for the different CMEM runs presented in the study including parameter values used for the calibration are summarized in Tab. 3. Model setup 'A' provides the first guess set up based on parametrizations and parameter values used in previous studies. The other three configurations outlined in Tab. 3 have been selected from more than 20 experiments.

Table 3: CMEM model setup for the calibration and validation computations. The  $h$  parameter is given in cm.

Setup	Roughness			Vegetation		
	Reference	Parameter	Value	Reference	Parameter	Value
A	Wigneron et al. (2001)	$h$	0.77	Jackson and Schmugge (1991)	$b_{forests}$	0.33
					$b_{C3/C4grass}$	0.20
					$b_{C3/C4crops}$	0.15
B	Wigneron et al. (2007)	$h_{baresoil}$	0.1	Wigneron et al. (2007)	$b'_{C3/C4grass}$	0.0375
		$h_{decid. forest}$	1.0		$b'_{C3/C4crops}$	0.05
		$h_{conif. forest}$	1.6		$b''_{C3/C4grass}$	0.05
		$h_{rain. forest}$	1.3		$b''_{C3/C4crops}$	0.0
		$h_{C3/C4grass}$	$f(\theta)$		$b'''_{C3/C4crops}$	0.7
		$h_{C3/crops}$	0.1			
		$h_{C4/crops}$	0.6			
C	Wigneron et al. (2001)	$h$	0.73	Kirдыashev et al. (1979)	$a_{geo}(high, low)$	0.33 / 0.66
D	Wigneron et al. (2001)	$h$	0.77	Kirдыashev et al. (1979)	$a_{geo}(high, low)$	0.33 / 0.33

## 5 Calibration and Validation

Skylab observations and the corresponding ERA-40 grid boxes are matched using the nearest neighbour technique. To produce a set of independent data pairs Skylab observations for a specific grid box were averaged. This is a reasonable approach since (i) the S-194 footprints are smaller than an ERA-40 grid box and (ii) averaging should be preferentially applied to brightness temperatures rather than geophysical parameters to avoid errors introduced through non-linearities in the radiative transfer calculation (Drusch et al. (1999a), Drusch et al. (1999b), Crow et al. (2001)). The spatial variability of the observations within each ERA-40 grid box has been used as a quality check for the observation / model data pair. Whenever the range of observed brightness temperatures for a specific grid box exceeded 10 K, the aggregated observation / model data pair is rejected. This test removes data pairs in coastal areas and grid boxes with large open water bodies, e.g. the Amazon, which may not be represented correctly in the ERA-40 data set.

Four tracks covering North and South America and including both winter and summer time passages have been selected for the CMEM calibration (Fig. 1 black tracks). The comparison between configuration 'A' brightness temperatures and the observations is shown in Fig. 2. The spatial distribution of brightness temperature differences (observation - model) shows a good coverage of calibration data for North America. In South America, one transect including the Amazon region and the Mato Grosso has been obtained. The differences for North America can be as large as 40 K and overall, the observed  $TB_{toa}$  are cooler than the corresponding model values. The maps suggest that the differences over the Eastern US are generally larger than over the Central and Western US. The scatter plots reveal a correlation of 0.52 and a bias of -8.4 K for the South America data (Fig. 3 b). The data pairs over North America exhibit a correlation of 0.34 and a bias of -8.4 K. The January 14

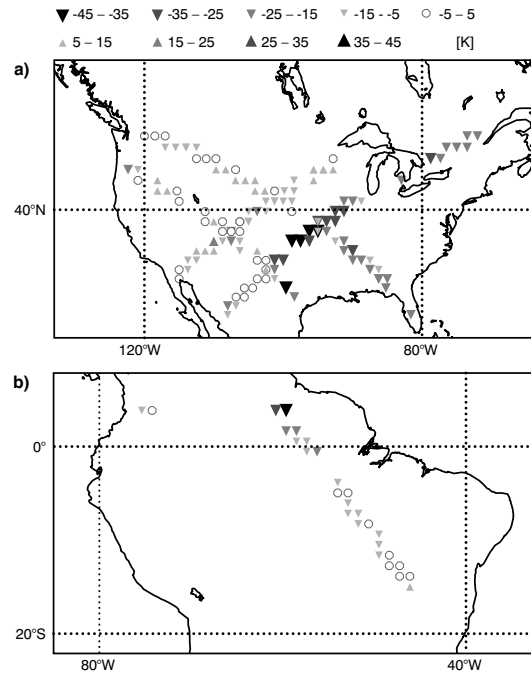


Figure 2: Differences between observed and modelled brightness temperatures ( $[obs - mod]$ ; CMEM setup 'A'; Tab. 1) for North America (a) and South America (b).

data present little bias (Fig. 3 a). This is somewhat surprising since large parts of the Western and Central US were snow covered during the overpass time and winter conditions are generally difficult to capture by emission models.

In total, ten combinations of different roughness and vegetation parameterizations have been used to compute brightness temperatures. For these computations the recommended parameter values from the reviewed literature have been applied. They are performed to gauge the output space and determine sensitivities. Set up 'B' is one example configuration, which gave promising results when data from field experiments were used (Wigneron et al. (2007)). In combination with the ECMWF model fields and the NWP auxiliary data sets the systematic and random errors are comparably large. For North America we obtain 0.04 and 23.1 K for the correlation coefficient and the bias, respectively (Fig. 3 c). The corresponding values for the South American data are 0.58 and 27.9 K (Fig. 3 d). The best results for both continents have been obtained using Wigneron et al. (2001) for describing the effects of surface roughness and Kirdyashev et al. (1979) for the parameterization of vegetation.

In the subsequent model runs the roughness height and the vegetation structure coefficient have been modified to fine tune CMEM. Figures 3 e) and f) show the brightness temperatures for configuration 'C' (Tab. 3). The correlations for North and South America have been increased and the biases of -1.2 K and -3.0 K are comparably low.

The vegetation structure coefficient in Eq. 9 should vary between 0.66 for a vegetation layer with elements in the form of small discs and 0.33 for cylinders. For configuration 'D'  $a_{geo}$  is set to 0.33 for low and high vegetation types (Fig. 3 g,h). For the North American data sets the correlation is 0.5 and the bias is -0.7 K. Over South America the modelled  $TB_{toa}$  are slightly too low when compared against the corresponding observations, the correlation is 0.56. However, this configuration leads to the best agreement between model based brightness temperatures and observations.

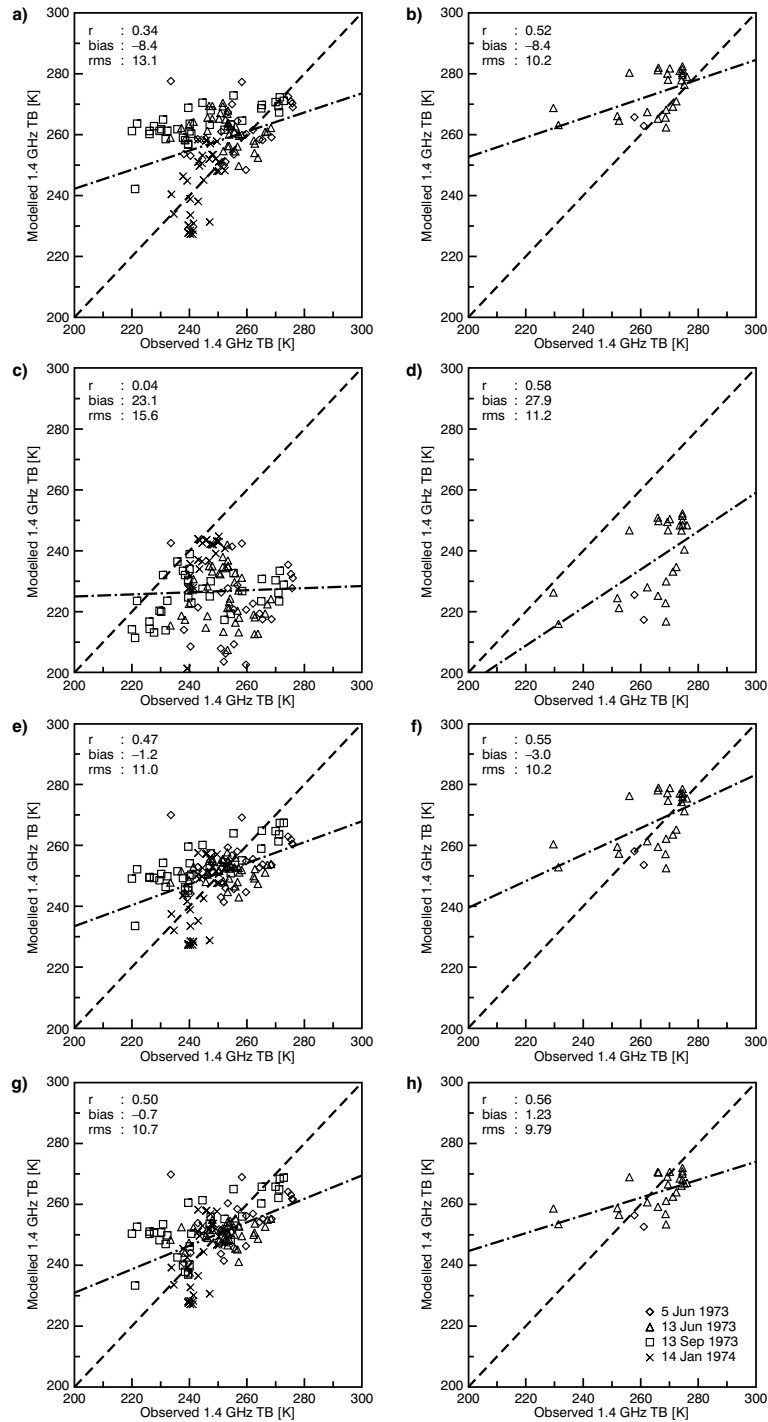


Figure 3: Differences between observed and modelled brightness temperatures for the CMEM configurations 'A' to 'D' (from top to bottom) as described in Tab. 1. Data for North America are shown on the left (a,c,e,g), data for South America are shown on the right (b,d,f,h). Different dates are represented through the symbols defined in h).

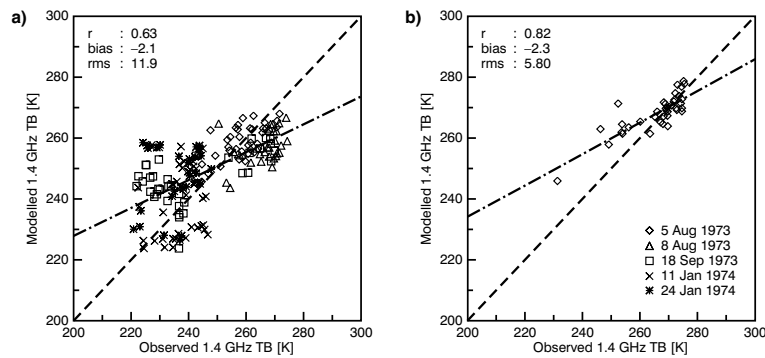


Figure 4: Validation results using configuration 'D' for (a) North America and (b) South America.

Observations from five overpasses (Fig. 1, grey tracks) have been used to validate CMEM setup 'D'. For three ERA-40 grid boxes over the Amazon region the modelled brightness temperatures are more than 16 K higher than the corresponding observations. The northern most data pair (Fig. 4 a,b) showing a difference of almost 20 K includes the 'Serra da Mocidade' plateau and the 'Rio Branco', the footprint further to the south is strongly influenced by the 'Rio Negro' and the most southern data pair is located over an extended swamp area, the 'Ilha Tupinambarama'. It is likely that these complex terrains with a significant amount of open and vegetation covered water bodies are not represented correctly by the land surface scheme in ERA-40. In general, the results for the validation data set are better than the ones obtained for the calibration data set indicating that the data sample size is too small to capture the full variability over the two continents. However, the results for the two data samples provide an estimate of the accuracy range that can be obtained with a continental scale calibration.

The calibration / validation experiments also show that it is not possible to reproduce the observed dynamical range of brightness temperatures. For the June, August and September dates the observed values range from 220 K to 275 K. The corresponding model data vary from 230 K to 265 K. We discuss this systematic difference and its implication for data assimilation applications in the following section.

## 6 Error Discussion

The weights of the observations and the model first guess in the analysis are determined through their respective error characteristics. The rms errors obtained in this study include both the first guess uncertainty and the observation error. Since the calibration error of the observations is below 1 K and the observations taken every 2.5 km along the orbit path are averaged to represent an ERA-40 grid box, it is assumed that the main contribution to the random errors originates from the model brightness temperatures.

Random errors in the ERA-40 soil moisture fields have been analysed using data from the Southern Great Plains Hydrology Experiment 1999. In general, root mean square errors varying from 2.5 % to 5 % have been found for dry and wet scenes, respectively (Drusch et al. (2004a)). Around selected Skylab overpasses gravimetric soil moisture samples were taken in Texas and Kansas. Details on the data, the field sites, and the synoptic situations can be found in Jackson et al. (2004). A comparison between spatially averaged in-situ measurements and the corresponding ERA-40 grid box values shows the systematic differences between soil moisture data sets (Fig. 5). The original in-situ observations comprise values from  $\sim 1$  to 51 % volumetric soil moisture resulting in area averages from 3 to 33 %. The dynamic range of the model is much smaller with a higher mean value. A first order correction for these systematic differences is a linear transformation to model

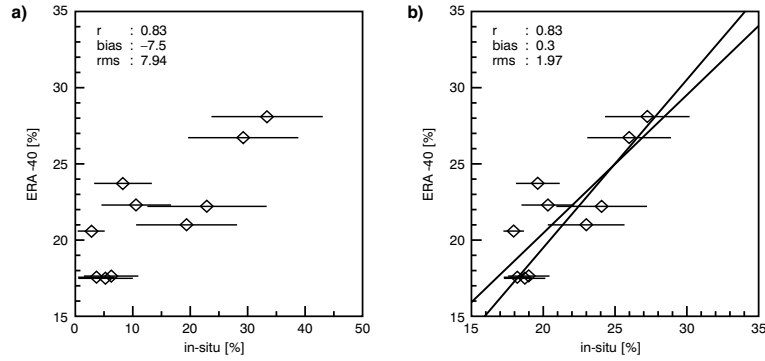


Figure 5: Spatially integrated volumetric soil moisture as obtained from in-situ measurements and the ERA-40 data set for ten days (a). Figure b) shows the in-situ observations after linear rescaling to the dynamic model range. Horizontal bars indicate the spatial variability ( $\pm$  one standard deviation).

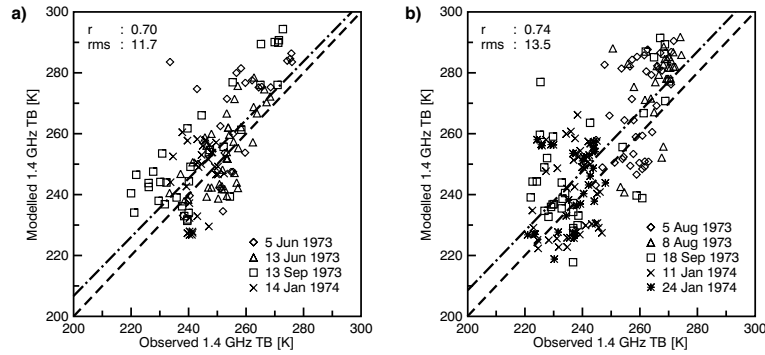


Figure 6: Calibration (a) and validation results (b) for configuration 'D' using re-scaled model fields (North America).

space:

$$\theta_{trans} = \theta_{pwp} + \frac{\theta_{in-situ}}{50} (\theta_{fc} - \theta_{pwp}) \quad (11)$$

with  $\theta_{pwp}$  and  $\theta_{fc}$  the model volumetric soil moisture at wilting point and field capacity, respectively,  $\theta_{in-situ}$  the original observation and  $\theta_{trans}$  the transformed value. This transformation reduces the bias to -0.3 % and results in a root mean square error of 1.97 % when compared against the model data (Fig. 5b). Over sparsely vegetated areas a 1% change in soil moisture results in a 2.5 K change in top of the atmosphere L-band brightness temperatures. Consequently, the random error in the ERA-40 soil moisture fields translates into brightness temperature uncertainties from 5 K (assuming a 2% error as obtained in Fig. 5b) to 12.5 K (for a 5% error obtained in Drusch et al. (2004a)).

Systematic differences between observations and the model background should be minimized prior to data assimilation applications to obtain statistically optimal analyses of soil moisture. Calibrating the forward operator reduces the bias between the modelled brightness temperatures and the observations. However, a systematic difference in the dynamic ranges of observed and predicted brightness temperatures remains.

Using Eq. 11 we transform the ERA-40 soil moisture data to the observed dynamic range and repeat the calibration and validation computations under configuration 'D' for North America. This simple correction results in a modelled variability that is almost identical with the observed one (Fig. 6). It should be noted that the bias after normalization is due to systematic differences between the in-situ measurements and the SKYLAB obser-

vations. An advanced bias correction scheme applied in brightness temperature space will effectively reduce any remaining systematic differences after CMEM calibration. In addition, the difference in the vertical resolution between the two data sets can result in brightness temperature uncertainty exceeding  $\pm 5$  K (Wilker et al. (2006)), which is included in the errors given in Figs. 2 and 3. Ideally, the top soil layer representing a depth of 1/10 of the wavelength should be discretized in more than 10 layers (Wilheit (1978)) to produce an accurate estimate of the soil dielectric constant.

Another major source of uncertainty is introduced through the vegetation data set. The ECOCLIMAP data used in the forward model represent an annual cycle but do not take interannual variability or variability on short time scales into account. In addition, ERA-40 adopted a different vegetation data set, which can lead to local inconsistencies with geophysical parameters, e.g. soil temperature. However, this is a common problem in many retrieval and forward modelling approaches where data sets from different sources necessarily are combined.

The observations over South America also reveal potential problems with the treatment of water bodies, i.e. lakes, rivers and swamps, in the NWP model fields and the microwave emission model. Although an accurate estimate of the fractional coverage of static open water can be obtained for each model grid box and satellite footprint from high resolution land cover data sets, it is hardly possible to determine the corresponding surface temperature and salinity. In ECMWF's IFS a model grid box is treated as land if the fractional coverage of water is less than 50 %. As a consequence, water bodies up to  $5500 \text{ km}^2$  can not be described correctly at ERA-40 resolution.

Potentially, the different spatial resolution of the satellite observations and the ERA-40 grid boxes and the matching procedure described above can introduce errors as well. To estimate the errors of the spatial aggregation procedure a subset of data pairs with ERA-40 grid boxes which are represented by at least 50 Skylab observations has been extracted. This number of observations results in a track of 125 km and ensures that the model grid box is well covered by measurements. The changes in rms errors and biases were marginal when only the subset of data pairs were analysed; the results and conclusions did not change.

## 7 ERA-40 Climatology

Based on the ERA-40 data set and CMEM a climatology for L-band brightness temperatures has been computed for the period 1990 to 2000. Mean values for July and the corresponding standard deviations are shown in Fig. 7. As one would expect, densely forested areas in the tropics and deserts are characterized by high brightness temperatures exceeding 280 K, wet areas and the Tibetan Plateau exhibits values around 230 K. It is interesting to note that the interannual variability is comparably small: large parts of the globe show values below 6 K. The tropical rainforest in the Amazon region is particularly stable and brightness temperature standard deviation is below 0.5 K. However, this area is comparably small and with the SMOS field of view exceeding 1000 km it remains questionable whether the rain forest could be used as a calibration target.

The mean annual cycle has been computed for North and South America (Fig. 8). Again, the interannual variability on the continental scale is low compared with the biases found in the calibration study. For North America the largest variability is found in winter time, which is probably related to the variability in snow. During summertime monthly mean brightness temperature variations hardly exceed 5 K. The values for South America are even lower due to the large coverage of tropical forests. The (calibrated) ERA-40 brightness temperature climatology will allow us to obtain a first check on the SMOS monitoring shortly after launch. However, comparisons should be based on large spatial scales only. Locally, the static ECOCLIMAP vegetation data base can introduce errors. Similar climatologies will be produced for different SMOS viewing angles and longer periods covering also the pre-satellite era.

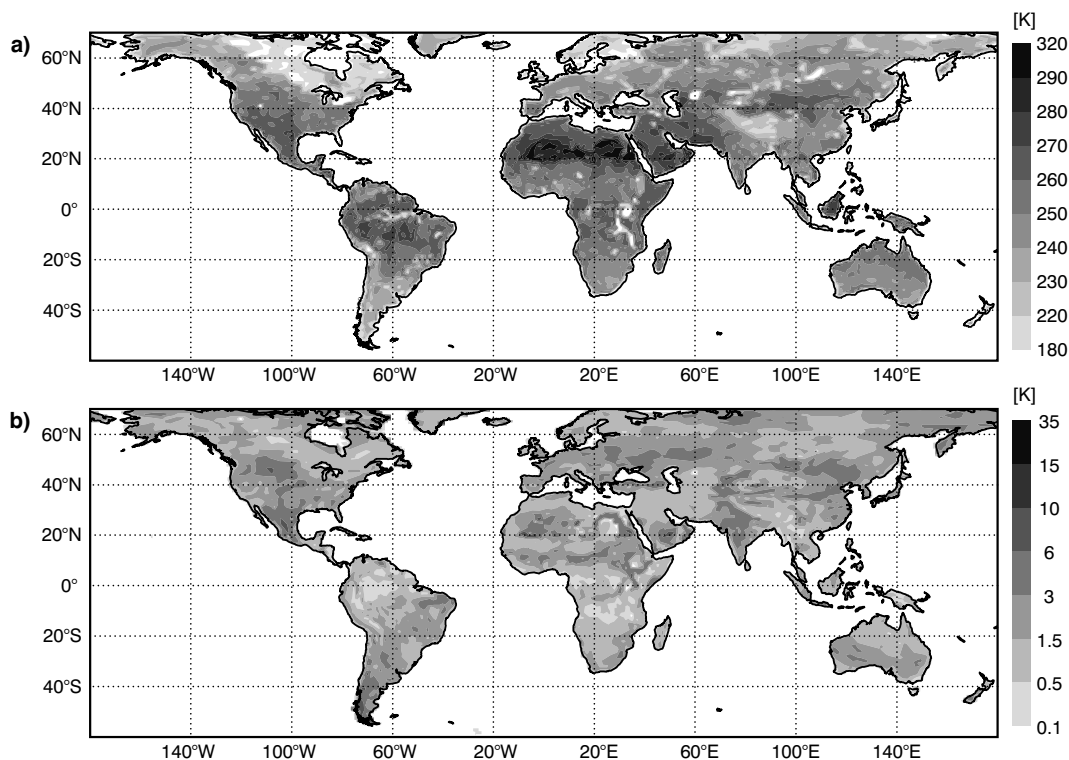


Figure 7: ERA-40 based L-band brightness temperatures at Nadir: (a) mean values for July 1990 - 2000 and (b) the corresponding standard deviation.

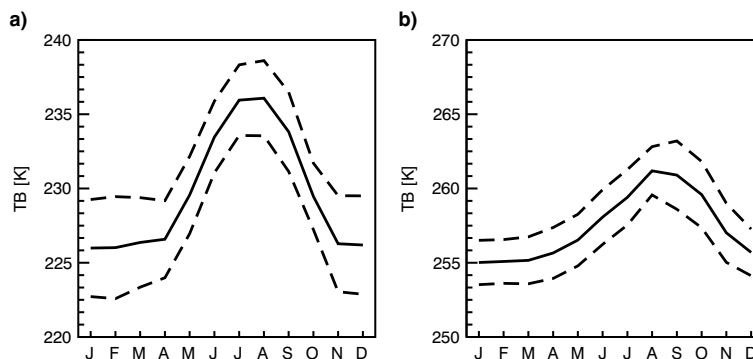


Figure 8: Mean annual cycle of L-band brightness temperatures at Nadir (thick lines) for the 1990 - 2000 period over (a) North America and (b) South America. The dashed lines indicate  $\pm$  one standard deviation.

## 8 Summary and Implementation Strategy

Apart from the S-194 data used in this study no spaceborne passive microwave L-band observations have been available on the continental scale. Parameterizations and coefficients for the land surface emissivity modelling have been derived from laboratory measurements and field experiments covering local to regional scales. In this study we focus on the continental scale due to the limited number of observations available and the coarse spatial resolution of the observations and the model fields. This study demonstrates that it is possible to calibrate a state-of-the-art emission model for NWP data assimilation applications and for operational soil moisture retrievals using the S-194 data.

However, backward and forward emission modelling both depend on a number of auxiliary data sets and geophysical parameters. Each of these data sets has systematic and random errors, which are difficult to quantify and which partly determine the choice of the parameterizations in the emission model, the value of a calibration parameter or the coefficients in a retrieval algorithm. For ECMWF's Integrated Forecast System configuration 'D' (Tab. 3) using parameterizations suggested by [Kirdyashev et al. \(1979\)](#) and [Wigneron et al. \(2001\)](#) gives the best results for the calibration and validation data sets. Our study demonstrates that it is important to develop new parameterizations not only on the local scale using high quality experimental data but also on larger scales with global data sets. CMEM is a convenient tool for these applications since it comprises a number of optional parameterizations and different I/O interfaces.

Within the Project for Intercomparison of Land-surface Parameterization Schemes (PILPS) it was shown that different land surface models can produce substantially different surface energy and water budgets even when they are driven by the same meteorological forcings ([Koster and Milly \(1997\)](#)). Consequently, model soil moisture is systematically different from satellite derived products and in-situ measurements representing the point scale. These systematic differences can not be avoided and are inherent to retrieval methods using auxiliary data sets and data assimilation applications alike. It has been shown that the bias between the model brightness temperatures and the observations can be minimized through the CMEM calibration. However, systematic differences in the brightness temperature dynamic range due to the model's soil moisture climatology remain present and have not been reduced.

Any systematic differences between the model and the observation should be minimized prior to data assimilation applications to obtain statistically optimal analyses. In the NWP community this pre-processing step is referred to as bias-correction. Various methods with different complexity levels have been applied in atmospheric data assimilation systems (e.g. [Dee and da Silva \(1998\)](#), [Harris and Kelly \(2001\)](#), [Auligne et al. \(2007\)](#)). For hydrological applications cumulative distribution function matching has been applied successfully ([Reichle and Koster \(2004\)](#), [Drusch et al. \(2005\)](#)). However, our comparison confirms that it will be necessary to develop bias correction methods for the assimilation of SMOS observations.

At ECMWF, CMEM will be implemented for the direct assimilation of brightness temperatures over snow-free areas. Near real time applications will have to be based on brightness temperatures: (i) the generation and acquisition of auxiliary data sets and the soil moisture retrieval itself will cause an unacceptable latency. (ii) The retrieved soil moisture product will be based on archived model fields, which are available at 3-hourly resolution. During the assimilation process the corresponding model fields are available every 12 minutes and should give more accurate estimates of the surface parameters, e.g. for the temperature fields, at a specific overpass time.

During the SMOS commissioning phase the SMOS data will be monitored operationally, e.g. model based brightness temperatures will be compared against the corresponding observations. The configuration will be based on the values and parameterizations defined in this study. It is envisaged that CMEM is updated 6 months after launch and a second calibration can be performed based on the observations available and the

latest results from the SMOS calibration / validation study. In the subsequent pre-operational phase the impact of SMOS observations on the forecast will be evaluated and it is planned to start with the operational application approximately 18 months after launch.

## Acknowledgements

The authors thank J.P. Wigneron for providing the original L-MEB FORTRAN code. S. Lafont (ECMWF) pre-processed the ECOCLIMAP data set. This work has been partly funded through EUMETSAT's Numerical Weather Prediction (NWP) Satellite application facility (SAF) visiting scientist program. We would like to thank E. Andersson (ECMWF) for his fruitful comments on the manuscript and Anabel Bowen and Rob Hine (both ECMWF) for their help with the preparation of the final figures.

## References

- Auligne, T., A. P. McNally, and D. P. Dee, 2007: Adaptive bias correction for satellite data in a numerical weather prediction system, *submitted to Quart. J. Roy. Meteorol. Soc.*.
- Balsamo, G., J.-F. Mahfouf, S. Bélair, and G. Deblonde, 2007: A land data assimilation system for soil moisture and temperature: An information content study, *J. Hydromet.*, **8**, 1225 – 1242.
- Choudhury, B., T. Schmugge, and T. Mo, 1982 : A parameterization of effective soil temperature for microwave emission. *J. Geophys. Res.*, pp. 1301–1304.
- Choudhury, B. J., T. J. Schmugge, A. Chang, and R. W. Newton, 1979: Effect of surface roughness on the microwave emission from soils, *J. Geophys. Res.*, **84**, 5699–5706.
- Crow, W.T., M. Drusch, and E.F. Wood, 2001: An observation system simulation experiment for the impact of land surface heterogeneity on AMSR-E soil moisture retrieval, *IEEE Trans. Geosc. Rem. Sens.*, **39**, 1622 – 1631.
- Dee, D. and A. da Silva, 1998: Data assimilation in the presence of forecast bias, *Quart. J. Roy. Meteorol. Soc.*, **124**, 269–295.
- Dobson, M.C., F.T. Ulaby, M.T. Hallikainen, and M. A. El-Rayes, 1985: Microwave dielectric behavior of wet soil - part II: Dielectric mixing models, *IEEE Trans. Geosc. Rem. Sens.*, **23**, 35–46
- Drusch, M., 2007: Initializing numerical weather prediction models with satellite derived surface soil moisture: Data assimilation experiments with ECMWF's Integrated Forecast System and the TMI soil moisture data set, *J. Geophys. Res.*, **112**, D03102, doi: 10.1029/2006JD007478
- Drusch, M. and S. Crewell, 2005: Radiative transfer, in *Encyclopaedia of Hydrological Sciences*, Wiley and Sons, UK, 13pp
- Drusch, M., E. Wood, and H. Gao, 2005: Observation operators for the direct assimilation of TRMM Microwave Imager retrieved soil moisture, *Geophys. Res. Lett.*, **32**, L19503, doi:10.1029/2005GL023623.
- Drusch, M., E. Wood, H. Gao, and A. Thiele, 2004a: Soil moisture retrieval during the Southern Great Plains hydrology experiment 1999: A comparison between experimental remote sensing data and operational products, *Wat. Res. Res.*, **40**, W0250410, doi:10.1029/2003WR002441.

- Drusch, M., D. Vasiljevic and P. Viterbo, 2004b: ECMWF's global snow analysis: Assessment and revision based on satellite observations, *J. Appl. Met.*, **43**, 1282–1294.
- Drusch, M., E. Wood, and T. Jackson, 2001: Vegetative and atmospheric corrections for soil moisture retrieval from passive microwave remote sensing data: Results from the Southern Great Plains Hydrology Experiment 1997, *J. Hydromet.*, **2**, 181–192.
- Drusch, M., E. Wood, and R. Lindau, 1999b: The impact of the SSM/I antenna gain function on land surface parameter retrieval, *Geophys. Res. Let.*, **26**, 3481–3484.
- Drusch, M., E. Wood, and C. Simmer, 1999a: Up-scaling effects in passive microwave remote sensing: ESTAR 1.4 GHz measurements during SGP97, *Geophys. Res. Let.*, **26**, 879–882.
- Eagleman, J.R. and W.C. Lin, 1976: Remote sensing of soil moisture by a 21-cm passive radiometer, *J. Geophys. Res.*, **81**, 3660–3666.
- FAO, 2000: Digital Soil Map of the World and Derived Soil Properties. Rev. 1. (CD Rom), 1, FAO Land and Water Digital Media Series. *available under <http://www.fao.org/ag/agl/agll/dsmw.htm>*
- Gao, H., E. Wood, T. Jackson, M. Drusch, and R. Bindlish, 2006: Using TRMM/TMI to retrieve soil moisture over the southern United States from 1998 to 2002, *J. Hydromet.*, **7**, 23–38.
- Harris, B. A. and G. Kelly, 2001: A satellite radiance-bias correction scheme for data assimilation, *Quart. J. Roy. Meteorol. Soc.*, **127**, 1453–1468.
- Haseler, J., 2004: Early-delivery suite, *Technical Memorandum 454*, [Available through ECMWF, Reading, UK], 35 pp.
- Hillel, D., 1980: Fundamentals of Soil Physics, *Academic Press, Inc. New York*, 413 pp
- Holmes, T., M. Drusch, J.P. Wigneron, and R. de Jeu, 2008: A global simulation of microwave emission: Error structures based on output from ECMWF's operational Integrated Forecast System, *IEEE Trans. Geosc. Rem. Sens.*, *in press*.
- Holmes, T., P. de Rosnay, R. de Jeu, J.-P. Wigneron, Y. H. Kerr, J.-C. Calvet, M.-J. Escorihuela, K. Saleh, and F. Lemaître, 2006 : A new parameterization of the Effective Temperature for L-band Radiometry. *Geophys. Res. Letters*, **33**,L07405, doi:10.1029/2006GL025724.
- Jackson, T.J., A.Y. Hsu, A. Van de Griend, and J.R. Eagleman, 2004: Skylab L-band microwave radiometer observations of soil moisture revisited, *Int. J. Rem. Sens.*, **25**, 2585–2606.
- Jackson, T.J., D.M. LeVine, A.Y. Hsu, A. Oldak, P.J. Starks, C.T. Swift, J.D. Isham, and M. Haken, 1999: Soil moisture mapping at regional scales using microwave radiometry: The Southern Great Plains Hydrology Experiment, *IEEE Trans. Geo. Rem. Sens.*, **37**, 2136–2151.
- Jackson, T., and T. Schmugge, 1991 : Vegetation effects on the microwave emission of soils. *Remote sens. environ.*, **36**,203–212.
- Jarlan, L., G. Balsamo, S. Lafont, A. Beljaars, J.C. Calvet and E. Mougin, 2008: Analysis of Leaf Area Index in the ECMWF land surface scheme and impact on latent heat and carbon fluxes: Application to West Africa, *submitted to J. Geophys. Res.*
- Jones, A.S., T. Vukicevic, and T.H. Vonder Haar, 2004: A microwave satellite observational operator for variational data assimilation of soil moisture, *J. Hydromet.*, **5**, 213–229.

- Kerr, Y.H. and E.G. Njoku, 1990: A semiempirical model for interpreting microwave emission from semiarid land surfaces as seen from space, *IEEE Trans. Geos. Remot. Sens.*, **28** (3), 384–393.
- Kirdyashev, K.P., A.A. Chukhlantsev and A.M. Shutko, 1979: Microwave radiation of the earth's surface in the presence of vegetation cover, *Radiotekhnika i Elektronika*, **24**, 256–264.
- Klein, L.A. and C.T. Swift, 1977: An improved model for the dielectric constant of sea water at microwave frequencies, *IEEE Trans. Antennas Prop.*, **25** (1), 104–111.
- Koster, R.D. and P.C.D. Milly, 1997: The interplay between transpiration and runoff formulations in land surface schemes used with atmospheric models, *J. Climate*, **10**, 1578–1591.
- Liebe, H., 2004 : MPM- An atmospheric millimeter-wave propagation model. *Int. J. Infrared Millimeter Waves*, **10**, 631–650.
- Masson, V., J.-L. Champeaux, F. Chauvin, C. Meriguet, and R. Lacaze, 2003: A global database of land surface parameters at 1-km resolution in meteorological and climate models. *J. Climate*, **16**, 1261–1282.
- Mironov, V., M. Dobson, V. Kaupp, S. Komarov, and V. Kleshchenko, 2004 : Generalized refractive Mixing dielectric model for moist soils. *Soil Sci. Soc. Am. J.*, **42**(4), 773–785.
- Njoku, E.G., T.J. Jackson, V. Lakshmi, T. Chan and S.V. Nghiem, 2003: Soil moisture retrieval from AMSR-E, *IEEE TGRS*, **41**, 215–229.
- Pellarin, T., J.-P. Wigneron, J.-C. Calvet, and P. Waldteufel, 2003: Global soil moisture retrieval from a synthetic L-band brightness temperature data set, *Journal of Geophysical Research (Atmospheres)*, **108**, 4364, doi:10.1029/2002JD003086.
- Pulliainen, J. T., M. T. Hallikainen, and J. Grandell, 1999: Hut snow emission model and its applicability to snow water equivalent retrieval, *IEEE Trans. Geos. Remot. Sens.*, **37**, 1378–1390.
- Reichle, R. and R.D. Koster, 2004: Bias reduction in short records of satellite soil moisture, *Geophys. Res. Lett.*, **31**, L19501, doi:10.1029/2004GL020938.
- Reichle, R. and R.D. Koster, 2005: Global assimilation of satellite surface soil moisture retrievals into the NASA catchment land surface model, *Geophys. Res. Lett.*, **32**, L02404, doi:10.1029/2004GL021700.
- Salgado, R., 1999: Global soil maps of sand and clay fractions and of the soil depth for MESONH simulation based on FAO/UNESCO soil maps, *CNRS/Meteo-France, Tech. Note*, **59**.
- Seuffert, G., H. Wilker, P. Viterbo, M. Drusch, and J. Mahfouf, 2004: On the usage of screen level parameters and microwave brightness temperature for soil moisture analysis, *J. Hydromet.*, **5**, 516–531.
- SMOS Expert Support Laboratories, 2007: SMOS level 2 processor for soil moisture algorithm theoretical based document (ATBD) *SO-TN-ESL-SM-GS-0001, issue 2.a*, p. 124.
- Ulaby, F.T., R.K. Moore, and A.K. Fung, 1982: Microwave remote sensing: Active and passive. Part 2. Radar Remote Sensing and Surface Scattering and Emission Theory, *Artech House*
- Ulaby, F.T., R.K. Moore, and A.K. Fung, 1986: Microwave remote sensing: From active to passive. Part 3. From theory to applications, *Artech House*
- Uppala, S.M., and 45 co-authors, 2005: The ERA-40 re-analysis, *Quart. J. Roy. Met. Soc.*, **131**, 2961–3012.

- van den Hurk, B.J.J.M., P. Viterbo, A.C.M. Beljaars, and A.K. Betts, 2000: Offline validation of the ERA40 surface scheme, *Technical Memorandum 295*, [Available through ECMWF, Reading, UK], 42pp.
- Wang, J.R. and B.J. Choudhury, 1981: Remote sensing of soil moisture content over bare field at 1.4 GHz frequency, *J. Geophys. Res.*, **86**, 5277–5282.
- Wang, J.R., and T. Schmugge, 1980 : An empirical model for the complex dielectric permittivity of soils as a function of water content. *IEEE Trans. Geosc. Remote Sens.*, **18**,288–295.
- Wegmüller, U., C. Mätzler, and E.G. Njoku, 1995: *Canopy opacity models*, in Passive Microwave Remote Sensing of Land-Atmosphere Interactions, Eds. B.J. Choudhury, Y.H. Kerr, E.G. Njoku and P.Pampaloni, VSP Utrecht, NL, 685 pp.
- Wegmüller, U. and C. Mätzler, 1999: Rough bare soil reflectivity model, *IEEE Trans. Geos. Remot. Sens.*, **37**, 1391–1395.
- Wigneron, J.P., L. Laguerre, and Y.H. Kerr, 2001: A Simple Parameterization of the L-band Microwave Emission from Rough Agricultural Soils, *IEEE Trans. Geos. Remot. Sens.*, **39**, 1697–1707.
- Wigneron, J.P., Y.H. Kerr, P. Waldteufel, K. Saleh, P. Richaume, P. Ferrazoli, M.-J. Escorihuela, J.P. Grant, B. Hornbuckel, P. de Rosnay, T. Pellarin, R. Gurney, and C. Mätzler, 2007: L-band Microwave Emission of the Biosphere (L-MEB) model: Results from calibration against experimental data sets over crop fields, *in press IEEE Trans. Geos. Remot. Sens.*
- Wilheit, T.T. 1978: Radiative transfer in a plane stratified dielectric, *IEEE Trans. Geos. Electr.*, **16**, 138–143.
- Wilker, H., M. Drusch, G. Seuffert, and C. Simmer, 2006: Effects of the near-surface soil moisture profile on the assimilation of L-band microwave brightness temperature, *J. Hydromet.*, **7**, 433–442.